A

Gene	Normal Lung	*Kras*^{G12D} *(KT)*	*Kras*^{G12D}*;p53*$^{\Delta/\Delta}$ *(KPT)*			
			Early	T_{nonMet}	T_{Met}	Met
Ampka1	14.67 ± 0.52	6.37 ± 0.92	6.66 ± 0.88	8.76 ± 1.76	10.58 ± 1.98	14.53 ± 3.61
Ampka2	6.30 ± 0.09	4.46 ± 0.42	4.51 ± 0.70	0.86 ± 0.48	0.90 ± 0.60	0.70 ± 0.72
Brsk1	0.76 ± 0.04	0.37 ± 0.07	0.41 ± 0.23	1.57 ± 0.64	1.67 ± 0.97	1.40 ± 0.91
Brsk2	3.72 ± 0.05	0.63 ± 0.14	0.83 ± 0.25	1.01 ± 0.32	0.74 ± 0.44	0.66 ± 0.73
Mark1	2.04 ± 0.16	0.21 ± 0.23	0.36 ± 0.16	0.20 ± 0.15	0.64 ± 0.92	1.51 ± 2.02
Mark2	50.95 ± 1.98	45.73 ± 1.59	47.52 ± 8.57	62.48 ± 9.08	55.02 ± 7.40	45.52 ± 15.97
Mark3	35.48 ± 1.07	15.30 ± 1.47	16.85 ± 3.00	24.11 ± 3.76	24.25 ± 3.31	31.14 ± 13.36
Mark4	31.72 ± 5.18	4.64 ± 1.26	4.98 ± 0.66	6.47 ± 1.41	7.51 ± 1.96	8.09 ± 2.68
Nuak1	6.66 ± 4.23	1.60 ± 0.46	1.72 ± 0.36	2.58 ± 0.81	2.63 ± 0.82	4.97 ± 1.99
Nuak2	26.81 ± 4.45	6.11 ± 1.77	4.81 ± 0.98	7.19 ± 1.98	6.26 ± 2.02	3.72 ± 3.35
Sik1	70.58 ± 9.79	35.56 ± 13.49	18.54 ± 0.50	25.68 ± 8.08	32.38 ± 18.23	21.67 ± 12.88
Sik2	23.31 ± 0.83	3.50 ± 1.60	2.38 ± 0.72	8.50 ± 3.62	8.00 ± 2.76	11.07 ± 2.89
Sik3	47.39 ± 2.87	14.82 ± 0.89	16.19 ± 1.84	19.81 ± 4.32	22.73 ± 4.46	27.46 ± 9.41

B

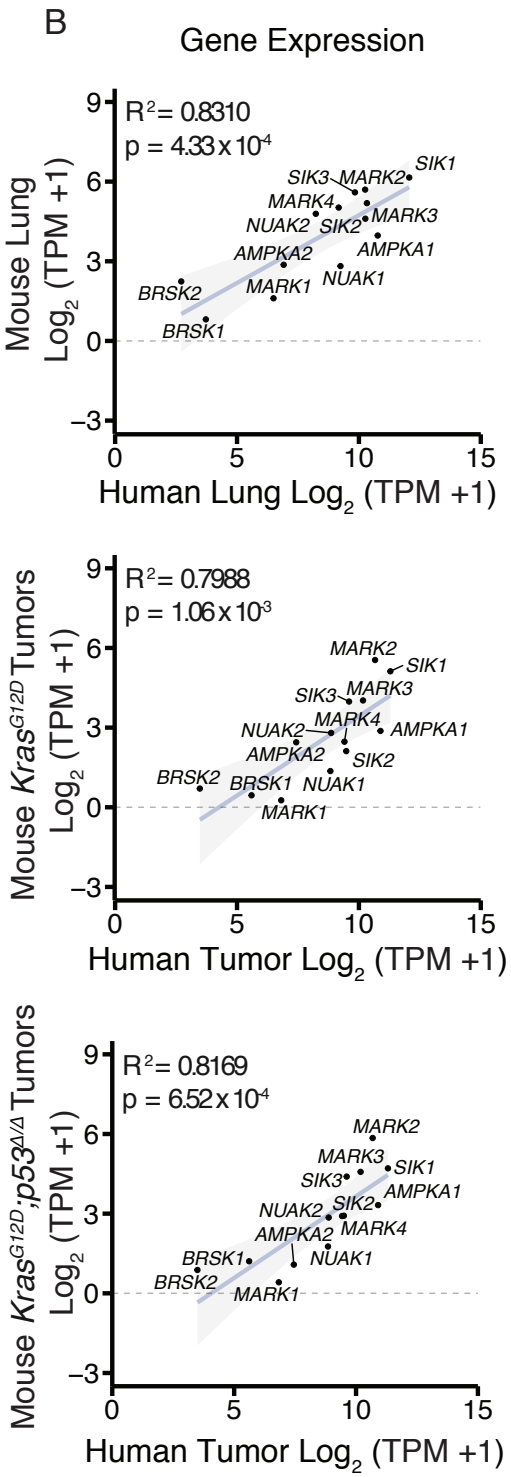

C

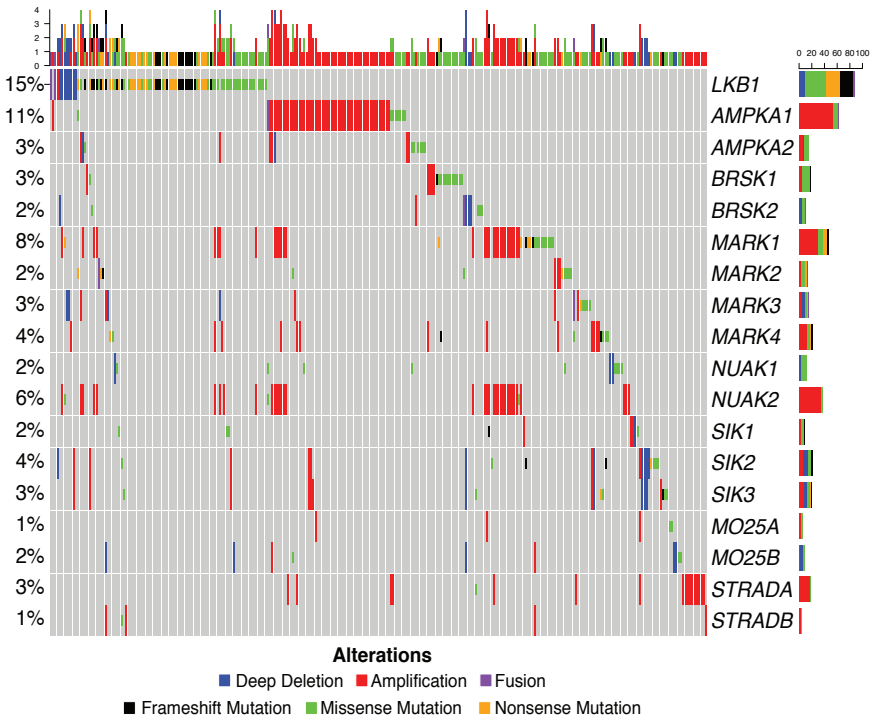

Supplementary Figure S1. mRNA expression and genomic alterations in LKB1 substrates in lung adenocarcinoma.
A. Expression of Lkb1 substrates (TPM) in normal lung and lung tumors from *Kras*$^{LSL\text{-}G12D/+}$*;R26*$^{LSL\text{-}Tomato}$ *(Kras*$^{LSL\text{-}G12D}$*,KT)* and Kras$^{LSL\text{-}G12D/+}$*;p53*^{floxflox}*;R26*$^{LSL\text{-}Tomato}$ *(Kras*^{G12D}*;p53*$^{\Delta/\Delta}$*, KPT)* mice. Mean expression +/- SD of each gene is indicated. *Kras*^{G12D}*;p53*$^{\Delta/\Delta}$ neoplastic cells are from early-stage lesions 2 months after initiation (Early), large non-metastatic primary tumors (T_{nonMet}), large metastatic primary tumors (T_{Met}) and metastases (Met) 6-9 months after tumor initiation (19). Substrates with average expression less than 2 are shown in gray.
B. Correlation of LKB1 substrate expression between human and mouse in normal lung and lung tumors. Expression levels within human tumors are compared to lung tumors from *KT* and *KPT* mice. Pearson correlation coefficient and associated p-value are indicated.
C. Oncoprint depicting the frequency and nature of genomic alterations in *LKB1*, its substrates, and its cofactors within human lung adenocarcinoma. *SIK2* and *SIK3* are adjacent in the genome, as are *MARK1* and *NUAK2* and hence copy number alterations often encompass both genes. Data obtained from the TCGA human lung adenocarcinoma provisional study (20).

A

sgRNA	Sequence
Ampkα1-sg7	CAAGGCTCCGAATCTTCTGC
Ampkα2-sg7	CCAATTGACAGGCCATAAAG
Mark2-sg1	AGTAAGTCCAACATGCTGCG
Mark3-sg2	ACACATCCTCACAGGCCGAG
Mark4-sg4	ATAGGCTGCTAAGGACCATC
Nuak1-sg4	GCGTCGCCCGAGATTGTCAA
Nuak2-sg2	GGATCTGCTGCACATACGGA
Sik1-sg2	GATCATGTCGGAGTTCAGTG
Sik1-sg1 (2nd)	TCTGGAGAAGATCTACCGGG
Sik2-sg7	TGATACAGTTTAATGATGTG
Sik3-sg3	TGGCAGAGAAGGAAGCTCGA
Sik3-sg1 (2nd)	GTTCAAACAGATCGTCACAG

B

	% indels
sgAmpkα1	27
sgAmpkα2	18
sgMark2	43
sgMark3	49
sgMark4	17
sgNuak1	41
sgNuak2	33
sgSik1	49
sgSik2	18
sgSik3	40
sgSik1 (2nd)	38
sgSik3 (2nd)	35

C

Dual Guide Vector

	% indels
sgControl/sgLkb1	66

D

Triple Guide Vector

	% indels		
Mark3/Mark2/Mark4	22%	23%	20%
Mark2/Mark4	26%	25%	
Mark3/Mark4	28%	27%	
Mark3/Mark2	27%	26%	
Mark2	27%		
Mark3	27%		
Mark4	25%		
Sik1/Sik2/Sik3	28%	22%	26%
Sik1	35%		
Sik2	27%		
Sik3	31%		

Supplementary Figure S2. Generation and *in vitro* validation of sgRNAs targeting Lkb1 substrates.
A. Sequences of the most efficient sgRNAs targeting each substrate. The second best sgRNA targeting *Sik1* and *Sik3* are also shown.
B. Lenti-sgRNA/Cre vectors with sgRNAs targeting each substrate lead to efficient indel generation in LSL-YFP;Cas9 cells in culture. The second best sgRNAs targeting *Sik1* and *Sik3* also generate high-frequency indels at their target sites and were used to confirm the tumor-suppressive effect of these kinases on lung tumor growth.
C. Efficient induction of indels in *Lkb1* using a previously published sgRNA that was subcloned into a vector to express both *sgLkb1* and a non-targeting sgRNA (68).
D. Indel detection rates within transduced cells are shown for each sgRNA in single, double, and triple U6-sgRNA vectors targeting members of the Mark and Sik families.

A

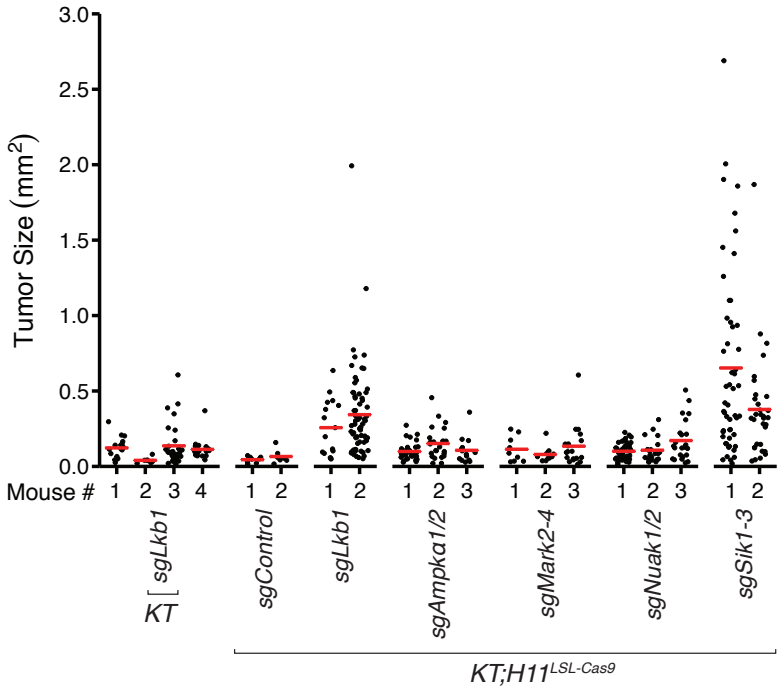

B

Sample	% indels *Ampkα1*	*Ampkα2*
Mouse1 Lobe	30	2
Mouse2 Lobe	28	69
Mouse3 Lobe	33	39
Mouse4 Lobe	35	41
Mouse5 Lobe	29	68

C

Sample	% indels *Nuak1*	*Nuak2*
Mouse1T1	32	40
Mouse1T2	83	43
Mouse2 Lobe	36	39
Mouse2 Lobe	92	40
Mouse2 Lobe	22	35

D

Sample	% indels *Mark2*	*Mark3*	*Mark4*
Mouse1T1	7	5	27
Mouse1 Lobe	7	12	18
Mouse2 Lobe	8	7	18

Supplementary Figure S3. Per-mouse tumor sizes and indel detection at targeted loci within tumors *in vivo*.
A. Tumor size data from individual *KT* and *KT;H11*$^{LSL\text{-}Cas9}$ mice with tumors initiated with the indicated Lenti-sgRNA/Cre vectors. Each dot represents a tumor and the crossbars indicate the mean. *KT;H11*$^{LSL\text{-}Cas9}$ mice with tumors initiated with *sgLkb1* and *sgSik1-3* Lenti-sgRNA/Cre vectors consistently develop larger tumors than those in control mice (*KT* mice with Lenti-sg*Lkb1*/Cre-initiated tumors and *KT;H11*$^{LSL\text{-}Cas9}$ mice with Lenti-sgControl/Cre-initiated tumors).
B-D. Analysis of indels at the targeted sites within FACS-isolated Tomato^{positive} neoplastic cells from tumors initiated in *KT;H11*$^{LSL\text{-}Cas9}$ mice with Lenti-sgRNA/Cre vectors targeting *Ampka1* and *Ampka2* (**B**), *Nuak1* and *Nuak2* (**C**), and *Mark2*, *Mark3*, and *Mark4* (**D**). Tumors in these mice were generally very small, therefore we isolated neoplastic cells from an entire lung lobe (Lobe). Cells isolated from individual tumors are indicated as "T". For all target genes, we detected inactivating indels, suggesting that inactivation of these genes leads to insufficient growth advantage to result in expansion within the timespan of this experiment.

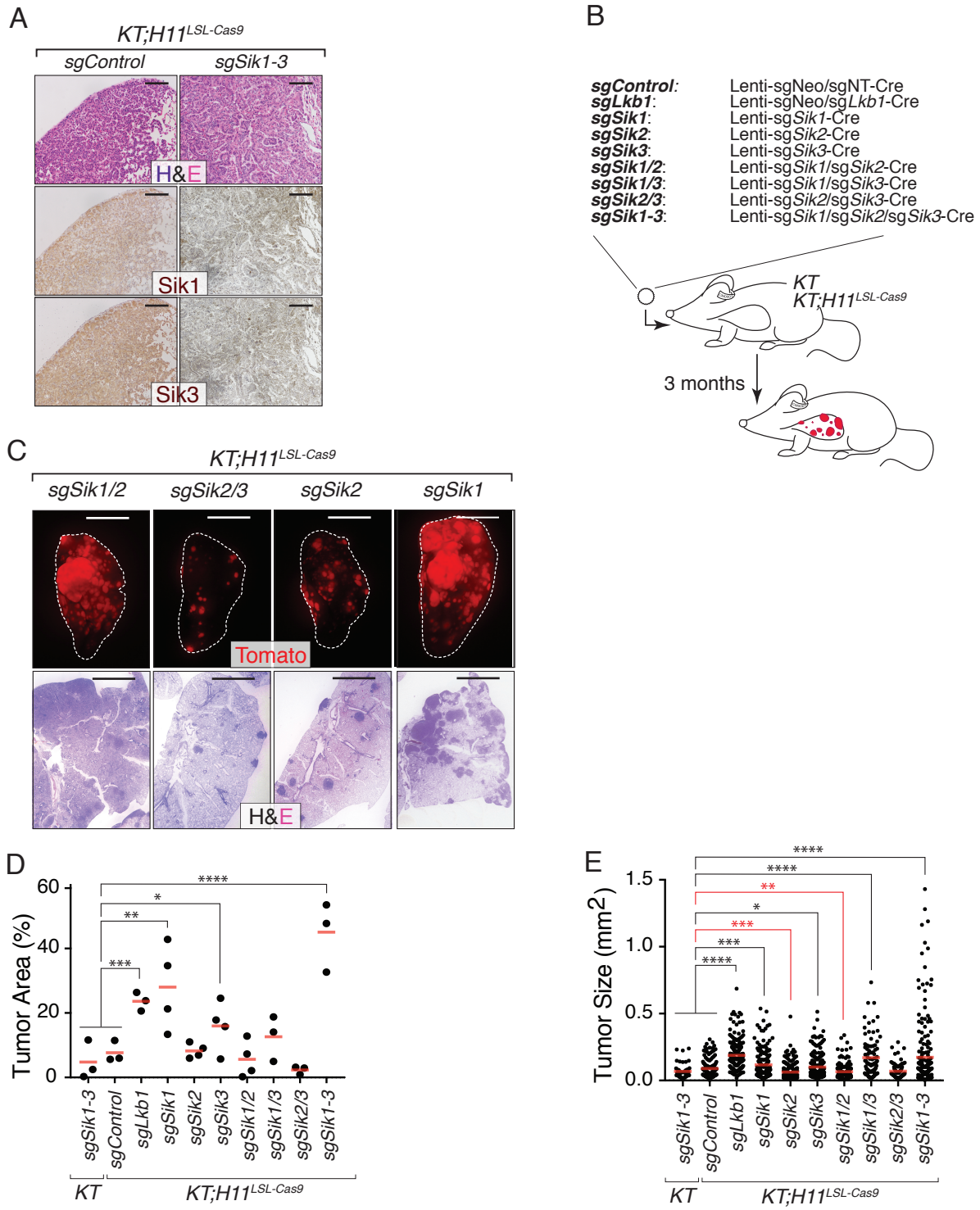

Supplementary Figure S4. Immunohistochemical evaluation of Sik1/3 ablation and analysis of tumor burden for deconvolution of Sik-mediated tumor suppression.

A. Representative immunohistochemistry for Sik1 and Sik3 on tumors generated in *KT;H11*$^{LSL\text{-}Cas9}$ mice with the indicated Lenti-sgRNA/Cre vectors. Scale bars = 100 μm.

B. Outline of the experiment to investigate tumor suppression mediated by each Sik paralog individually and in combinations. Tumors were initiated in *KT* and *KT;H11*$^{LSL\text{-}Cas9}$ mice with the indicated lentiviral sgRNA/Cre vectors.

C. Representative fluorescence (top) and H&E (bottom) images of lungs from *KT;H11*$^{LSL\text{-}Cas9}$ mice with tumors initiated with Lenti-sgRNA/Cre vectors indicated. Lung lobes are outlined with a white dashed line. Top scale bars = 5 mm. Bottom scale bars = 2 mm.

D-E. Tumor area (**D**) and size (**E**) from histology in *KT;H11*$^{LSL\text{-}Cas9}$ mice with tumors initiated with Lenti-sgRNA/Cre as indicated. In D, each dot corresponds to a mouse. In E, each dot indicates a tumor. Crossbars indicate the mean. Red significance bars indicate instances in which a given genotype yields tumors that are smaller than control tumors. * p-value < 0.05, ** p-value < 0.01, ***p-value < 0.001, ****p-value <0.0001.

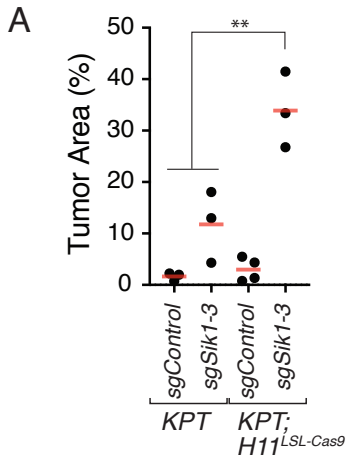

B

Tissue	% indels *Sik1*	*Sik2*	*Sik3*
2308T3	**84**	4	25
2308T4	6	8	**82**
2308T5	**38**	8	**40**
2308T6	3	3	10
2308T7	31	1	**44**
2308T8	27	6	**80**
2544_DTC	**40**	7	**97**
2544_Met	**47**	4	**71**

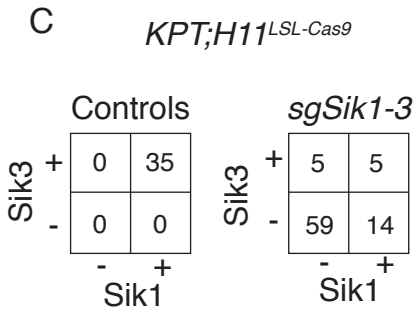

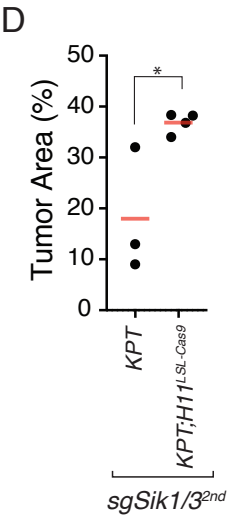

Supplementary Figure S5. Inactivation of Sik1 and/or Sik3 increases tumor burden in a p53-deficient context.
A. Tumor area from histology on lungs from *KPT* and *KPT;H11*$^{LSL\text{-}Cas9}$ mice with tumors initiated with the indicated Lenti-sgRNA/Cre vectors. Each dot represents a mouse. Crossbars indicate the mean.
B. Percent indels in *Sik1*, *Sik2*, and *Sik3* in cancer cells sorted from individual Lenti-sg*Sik1-3*/Cre initiated tumors from *KPT;H11*$^{LSL\text{-}Cas9}$ mice. DTC; sorted disseminate tumors cells from the pleural cavity. Met; metastasis.
C. Immunohistochemistry for Sik1 and Sik3 on tumors from control mice (*KPT* mice with Lenti-sg*Sik1-3*/Cre-initiated tumors and *KPT;H11*$^{LSL\text{-}Cas9}$ mice with Lenti-sgControl/Cre-initiated tumors) and *KPT;H11*$^{LSL\text{-}Cas9}$ mice with Lenti-sg*Sik1-3*/Cre-initiated tumors.
D. Tumor area from histology on lungs from *KPT* and *KPT;H11*$^{LSL\text{-}Cas9}$ mice with tumors initiated with Lenti-sg*Sik1/3*^{2nd}/Cre vectors as indicated. Each dot represents a mouse. Crossbars indicate the mean. An independent set of sgRNAs targeting *Sik1* and *Sik3* was used. * p-value < 0.05, ** p-value < 0.01, ***p-value < 0.001, ****p-value <0.0001.

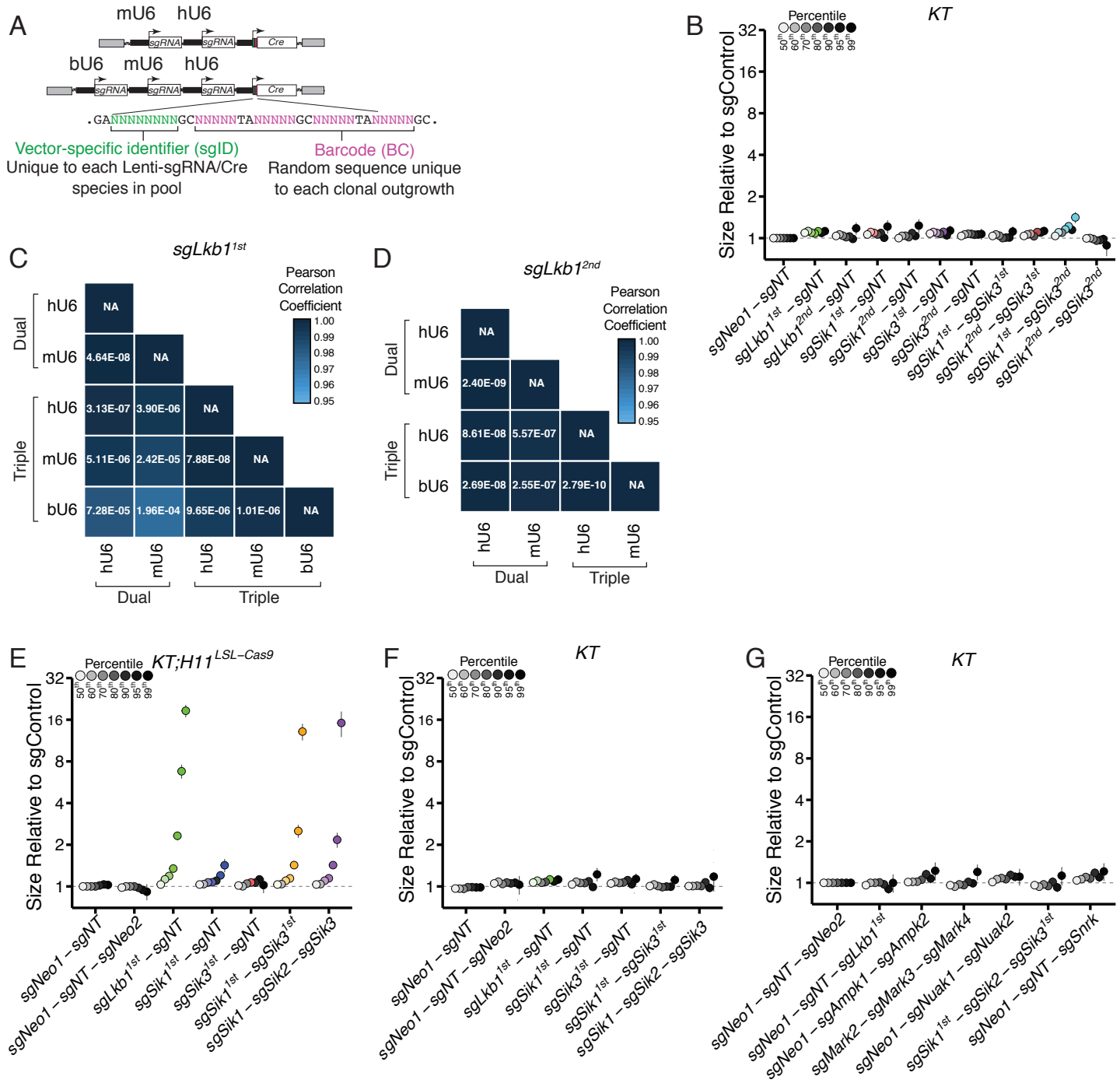

Supplementary Figure S6. Lentiviral vector barcode design and a lack of added growth advantage resulting from *SIK2* targeting.
A. Sequence-level view of sgRNA identifier (sgID; green) and random barcode (BC; pink) modules incorporated within Lenti-sgRNA/Cre vectors to enable labeling of transduced cells with a vector-specific identifier to enable stratification of tumors by genotype and clonal identifier to uniquely label individual tumors.
B. Representation of a subset of the pool of vectors targeting *Sik1* and/or *Sik3* in *KT* mice, where Cas9 is not present to disrupt targeted loci. Relative size of tumors at the indicated percentiles is merged data from five mice at 16 weeks post-initiation, normalized to the size of sgNeo1-sgNT tumors. Error bars denote 95% confidence intervals determined by bootstrap sampling. Percentiles that are significantly different from sgNeo-sgNT are in color.
C,D. Heatmaps depicting the correlation across percentiles between tumor size distributions resulting from *Lkb1* targeting using one of two independent sgRNAs at different possitions within the dual or triple sgRNA vectors. P-values are listed within individual tiles.
E,F. Quantitative analysis of the impact of *Sik2* targeting in addition to Sik1 and Sik3 ablation. Relative size of tumors at the indicated percentiles is merged data from 10 *KT;H11*$^{LSL\text{-}Cas9}$ mice (**E**) or five *KT* mice (**F**), normalized to the size of sgNeo1-sgNT and sgNeo1-sgNT-Neo2 tumors. Error bars denote 95% confidence intervals determined by bootstrap sampling. Percentiles that are significantly different from inert vectors are in color.
G. Representation of a subset of the pool of vectors targeting Lkb1 substrates in *KT* mice. Relative size of tumors at the indicated percentiles is merged data from five mice at 16 weeks post-initiation, normalized to the size of sgNeo1-sgNT-sgNeo2 tumors. Error bars denote 95% confidence intervals determined by bootstrap sampling. Percentiles that are significantly different from sgNeo-sgNT-sgNeo2 are in color.

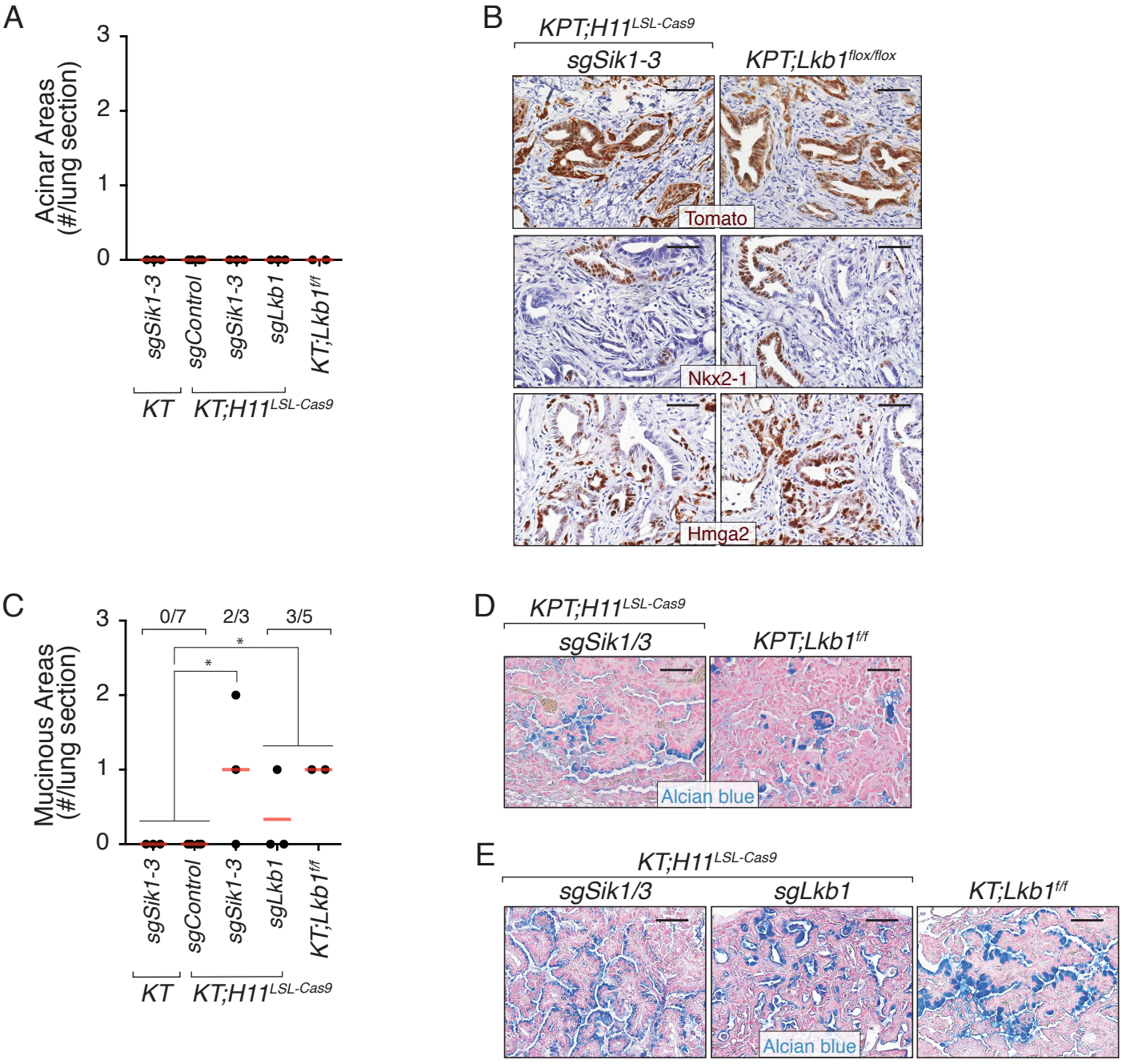

Supplementary Figure S7. Sik-targeted lung tumors develop large adenocarcinoma areas with acinar histology and focal areas with mucinous differentiation that are not present in *K* and *KP* models.

A. No acinar lesions were detected in models in which p53 remained intact. Number of large, highly stromalized, acinar areas per lung section from the indicated genotypes of mice. Each dot represents a mouse and the crossbar is the mean.

B. Cancer cells, marked by the *R26*$^{LSL\text{-}Tomato}$ Cre-reporter, form malignant glandular structures as well as small nests and single cancer cells within the stroma. Cancer cells within these regions of Sik-targeted and Lkb1-deficient tumors exhibit heterogeneous expression of Nkx2-1 and Hmga2. Scale bars = 50 μm.

C. Number of areas with alcian blue-positive cancer cells in lung sections from the indicated genotypes of mice. Each dot represents a mouse and the crossbars indicate the mean. The fraction of mice with control, Sik-targeted, and Lkb1-deficient tumors harboring one or more mucinous areas is shown above the plot. * p-value < 0.05.

D. Additional images of areas of lung tumors with mucinous differentiation and abundant intracellular mucin. Genotypes of mice are indicated. Alcian blue stains mucin. Scale bars = 50 μm.

E. Representative histology of areas of p53-proficient lung tumors with mucinous differentiation and abundant intracellular mucin. Genotypes of mice are indicated. Alcian blue stains mucin. Scale bars = 50 μm.

A

	Mouse Genotype	Viral vector	p63+		Ck5+	
KP controls	*KP* (N=3)	Lenti-Cre	0/91	0/150	0/65	0/128
	KPT (N=2)	*sgSik1-3*	0/18		0/21	
	KPT;H11$^{LSL\text{-}Cas9}$ (N=2)	*sgControl*	0/41		0/42	
KP;Sik-targeted	*KPT;H11*$^{LSL\text{-}Cas9}$ (N=3)	*sgSik1-3*	0/120	0/263	0/98	0/255
	KPT;H11$^{LSL\text{-}Cas9}$ (N=4)	*sgSik1/3*	0/143		0/157	
	KPT;Lkb1$^{f/f}$ (N=3)	Lenti-Cre	0/135		0/117	

B

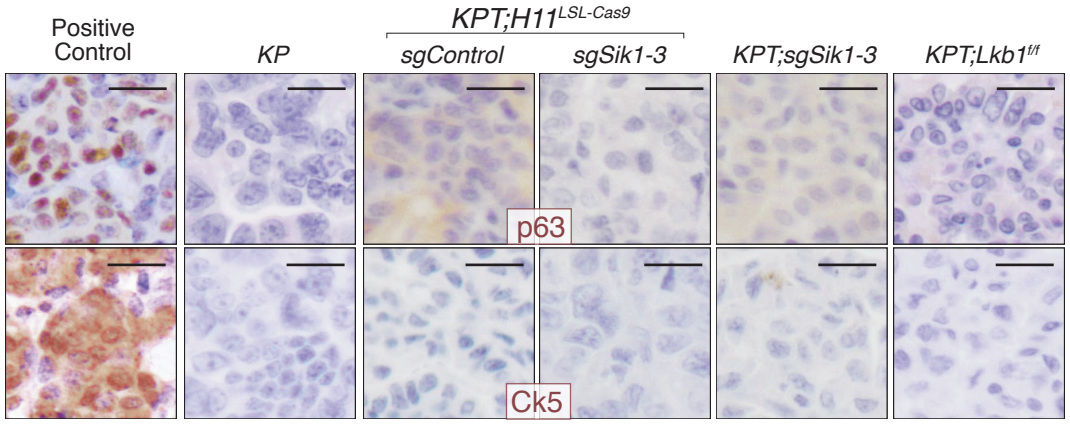

C

	Mouse Genotype	Viral vector	p63+		Ck5+	
K controls	*KT* (N=2)	*sgSik1-3*	0/84	0/119	0/73	0/103
	KT;H11$^{LSL\text{-}Cas9}$ (N=2)	*sgControl*	0/35		0/30	
	KT;H11$^{LSL\text{-}Cas9}$ (N=5)	*sgSik1-3*	0/275		0/247	
	KT; Lkb1$^{f/f}$ (N=4)	Lenti-Cre	0/181		0/207	

D

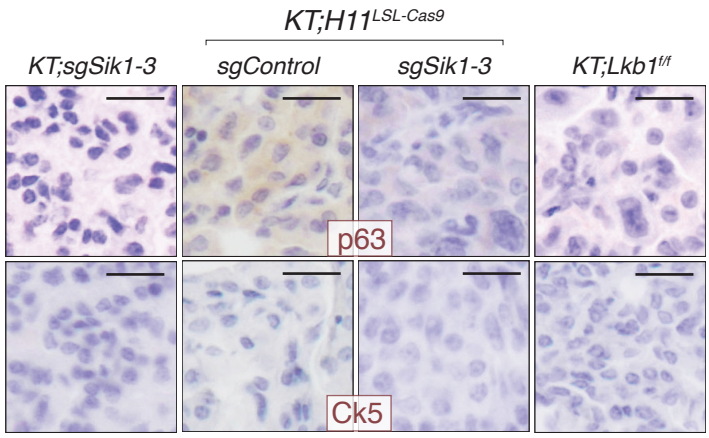

Supplementary Figure S8. Absence of squamous cell carcinoma in Lkb1-deficient and Sik-targeted tumors.
A. Neither Lkb1-deficient nor Sik-targeted Kras^{G12D};p53-deficient (*KP*) tumors express canonical markers of lung squamous cell carcinoma (p63 and Ck5). Mouse genotype, cohort size, and viral vector used for tumor initiation is indicated. The number of p63- or Ck5-positive tumors/total number of tumors analyzed is shown. In cases where multiple groups of mice ultimately generate the same genotype of tumors (ex. *KP* controls), the aggregate number of p63- and Ck5-positive tumors/total number of tumors analyzed is shown.
B. Representative p63 and Ck5 immunohistochemisty images from tumors in the indicated genotypes of mice initiated with the indicated lentiviral vectors. Scale bar = 50μm. Positive control sections are from a *Kras*$^{LSL\text{-}G12D/+}$;*Lkb1*$^{flox/flox}$ mouse with Adenoviral-Cre-initiated tumors (kindly provided by Dr. Kwok-Kin Wong's laboratory).
C. Neither Lkb1-deficient nor Sik-targeted Kras^{G12D} (*K*) tumors express canonical markers of lung squamous cell carcinoma (p63 and Ck5). The mouse genotype, number of mice in each group, and viral vector used for tumor initiation is indicated. The number of p63- or Ck5-positive tumors/total number of tumors analyzed is shown. In cases where multiple groups of mice ultimately generate the same genptype of tumors (ex. *K* controls) the aggregate number of p63- and Ck5-positive tumors/total number of tumors analyzed is shown.
D. Representative p63 and Ck5 immunohistochemistry images from tumors in the indicated genotypes of mice initiated with the indicated lentiviral vectors. Scale bar = 50μm.

A

Tumor	Mutated Read Fraction *Sik1*	*Sik2*	*Sik3*
KT;H11^{Cas9} sgSik1 #1	2/3	N/A	N/A
KT;H11^{Cas9} sgSik1 #2	8/9	N/A	N/A
KT;H11^{Cas9} sgSik1 #3	16/16	N/A	N/A
KT;H11^{Cas9} sgSik1-3 #1	8/9	0/0	0/0
KT;H11^{Cas9} sgSik1-3 #2	6/7	0/0	0/0

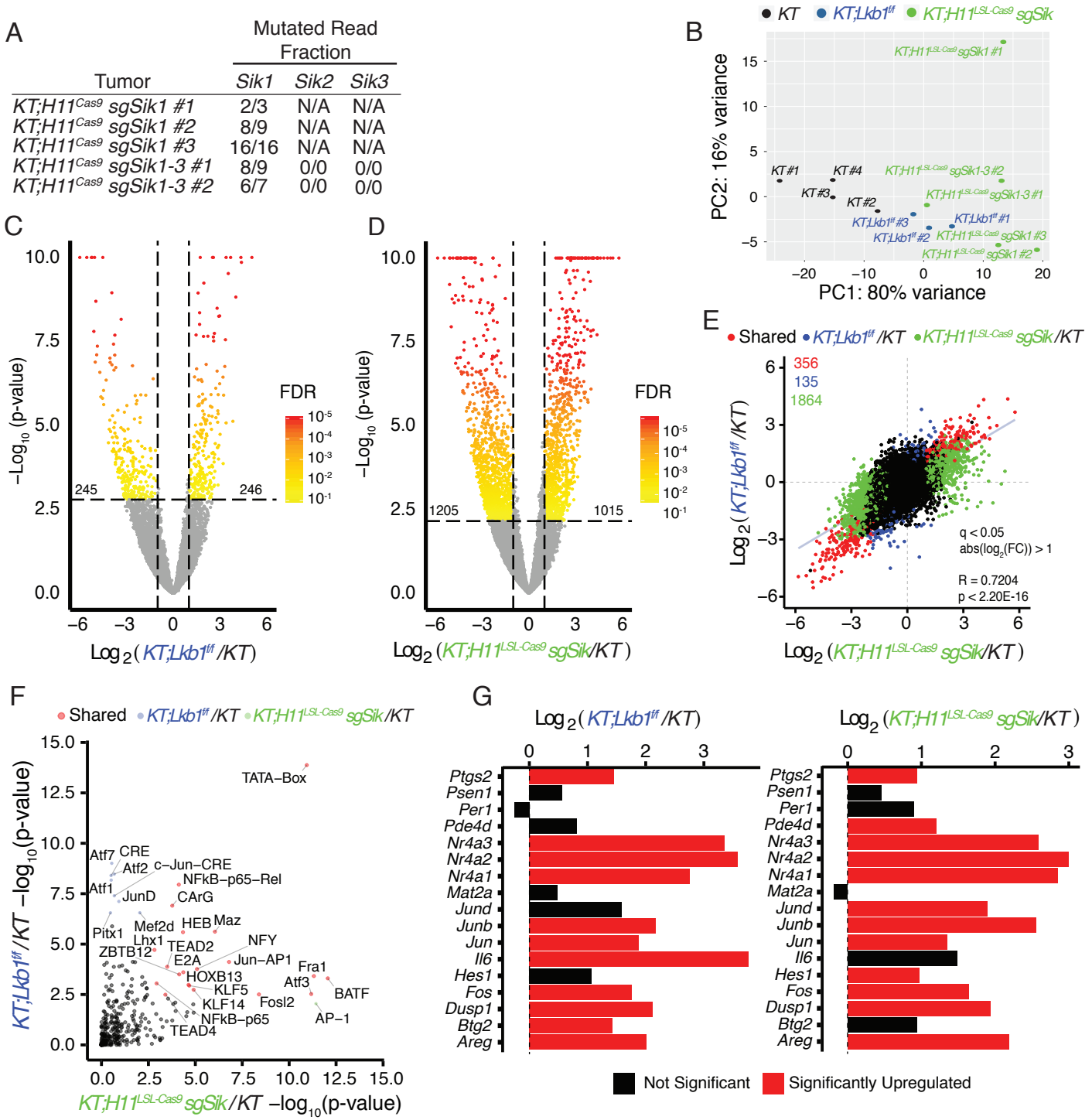

Supplementary Figure S9. Overlapping transcriptional states between Sik and Lkb1 deficiency including upregulation of Creb-driven transcriptional programs.

A. Indel analysis at *Sik1/2/3* from aligned RNA-seq reads derived from tumors initiated by Lenti-sg*Sik*/Cre in *KT;H11$^{LSL-Cas9}$* mice. Indel frequency reported in terms of the fraction of reads overlapping the sgRNA PAM and seed sequences that are mutated. N/A indicates that indels at these loci were not surveyed given that they were not targeted by the indicated Lenti-sgRNA/Cre vectors/

B. Principal component analysis of tumors derived from *KT* and *KT;Lkb1$^{flox/flox}$* mice as well as *KT;H11$^{LSL-Cas9}$* mice transduced with lentiviral sgRNA vectors targeting either *Sik1* alone or *Sik1-3*.

C,D. Volcano plots depicting global overview of differential gene expression in *KT;Lkb1$^{flox/flox}$* and *KT;H11$^{LSL-Cas9}$* sgSik tumors relative to *KT* tumors. Significant differential expression is defined as an absolute $\log_2$(Fold Change) > 1 and q < 0.05.

E. Comparison of differential gene expression in *KT;Lkb1$^{flox/flox}$* and *KT;H11$^{LSL-Cas9}$* sgSik tumors relative to *KT* tumors at the gene level. Significantly differentially expressed genes that are unique to either tumor genotype or shared is indicated by dot color.

F. Motif enrichment at the promoters of genes upregulated in *KT;Lkb1$^{flox/flox}$* and *KT;H11$^{LSL-Cas9}$* sgSik tumors relative to *KT* tumors. Bi-plot depicts those transcription factor motifs that are significantly enriched in either or both *KT;Lkb1$^{flox/flox}$* and *KT;H11$^{LSL-Cas9}$* sgSik tumors. Each dot corresponds to a transcription factor motif and the color indicates whether the motif is unique or shared.

G. Expression of prototypical Creb target genes in *KT;Lkb1$^{flox/flox}$* and *KT;H11$^{LSL-Cas9}$* Lenti-sg*Sik*/Cre tumors relative to *KT* tumors (41-43). Significant upregulation is defined as $\log_2$(Fold Change) > 0 and q < 0.05.

A

Model Comparison	Gene Set	NES	FDR	Source
K;Lkb1$^{f/f}$*/K*	Higher in Sik Deficiency	2.97	0.000	Carretero *et al.*, 2010
K;Lkb1$^{f/f}$*/K*	Lower in Sik Deficiency	-1.97	0.000	Carretero *et al.*, 2010
K;Lkb1$^{f/f}$*/K*	Higher in Sik Deficiency	2.54	0.000	Ji *et al.*, 2007
K;Lkb1$^{f/f}$*/K*	Lower in Sik Deficiency	-1.31	0.091	Ji *et al.*, 2007
K;Lkb1$^{f/f}$*/K;p53*$^{f/f}$	Higher in Sik Deficiency	2.73	0.000	Nagaraj *et al.*, 2017
K;Lkb1$^{f/f}$*/K;p53*$^{f/f}$	Lower in Sik Deficiency	-2.34	0.009	Nagaraj *et al.*, 2017
K;Lkb1$^{f/f}$*/K;p53*$^{f/f}$	Higher in Sik Deficiency	2.08	0.000	Ji *et al.*, 2007
K;Lkb1$^{f/f}$*/K;p53*$^{f/f}$	Lower in Sik Deficiency	1.45	0.009	Ji *et al.*, 2007
K;Lkb1$^{f/f}$*/K;p16*$^{Ink4a-/-}$	Higher in Sik Deficiency	2.62	0.000	Ji *et al.*, 2007
K;Lkb1$^{f/f}$*/K;p16*$^{Ink4a-/-}$	Lower in Sik Deficiency	-1.76	0.000	Ji *et al.*, 2007

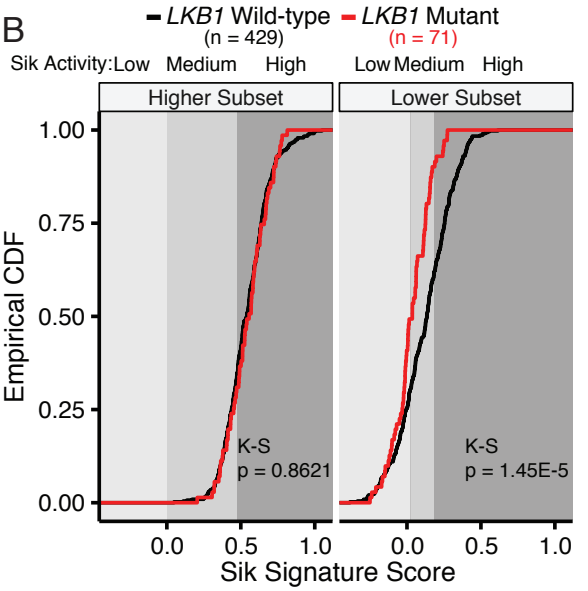

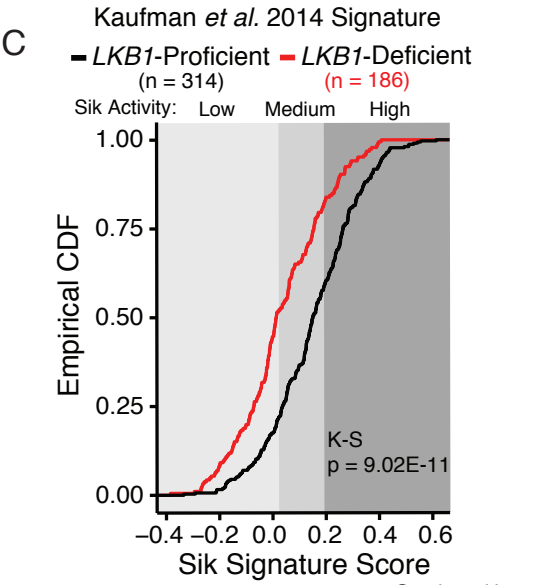

Gene Set	Size (Genes)	Overlap with Kaufman Signature
Higher in Sik Deficiency	340	4
Lower in Sik Deficiency	643	0
Kaufman Signature	16	N/A

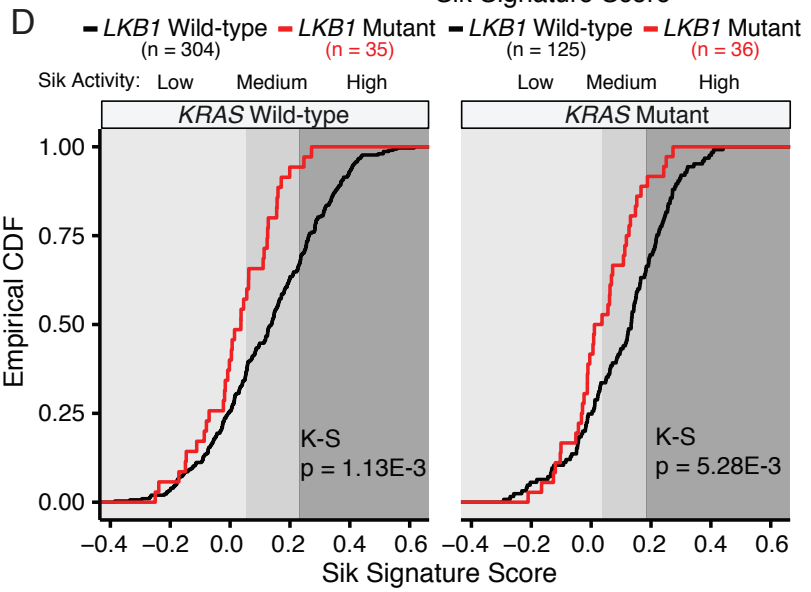

E

Sik Signature Bin	*Sik1* Mutant	*Sik3* Mutant	Putative Passenger *Sik1* Mutant	Putative Passenger *Sik3* Mutant
Low	1	3	2	3
Medium	1	2	0	0
High	0	2	0	0

F

Comparison (*LKB1* Genotypes)	Gene Set	NES	FDR	Source
Mutant (n = 8) / Wild-type (n = 48)	Lower in Sik Deficiency	-1.87	0.000	Selamat *et al.*, 2012
Mutant (n = 6) / Wild-type (n = 75)	Lower in Sik Deficiency	-1.99	0.000	Wilkerson *et al.*, 2012
Mutant (n = 68) / Wild-type (n = 374)	Lower in Sik Deficiency	-1.84	0.000	Schabath *et al.*, 2016
Mutant (n = 13) / Wild-type (n = 23)	Lower in Sik Deficiency	-2.16	0.000	Skoulidis *et al.*, 2015
Mutant (n = 15) / Wild-type (n = 25)	Lower in Sik Deficiency	-1.43	0.089	Schliekelman *et al.*, 2015

Supplementary Figure S10. A signature of Sik loss is enriched in LKB1-deficient lung adenocarcinoma in humans and mice.
A. GSEA using subsets of upregulated or downregulated genes in the absence of Sik performed on gene expression data from various genetically engineered mouse models of lung adenocarcinoma (7,14,29).
B. Separation of Sik signature into subsets of genes that are either upregulated or downregulated in Sik-targeted tumors relative to Sik-proficient *KT* tumors. Comparison of each subsetted signature with the entire to signature comprised of all differentially expressed genes in the Sik-targeted state. Background shading delineates the Sik signature score tertiles.
C. Sik signature score distributions for human lung adenocarcinomas classified as either *LKB1*-proficient or deficient using a signature of LKB1 loss comprised of FOX/CREB-regulated genes that are upregulated in LKB1-deficient human tumors (7). The extent of overlap between signatures is indicated in table. Given the opposite directionality of the lower in Sik Deficiency and Kaufman signatures, there is no overlap. The lack of overlap between the Kaufman signature and genes higher in Sik Deficiency is consistent with the modest overlap of upregulated genes between *KRAS* mutant, LKB1-deficient human lung tumors and mouse models thereof (7).
D. Examination of the Sik signature score distributions for *LKB1* wild-type versus mutant tumors that do or do not harbor mutant *KRAS*.
E. Summary of the stratification of human lung adenocarcinoma samples bearing mutations in either *Sik1* or *Sik3* mutations across the three tertiles defined by the Sik signature. Patients are further broken down on the basis of whether the mutation is predicted to be a passenger. Those patients bearing coincident mutations in *LKB1* are excluded from this table.
F. Summary of GSEA results in lung adenocarcinoma patients and cell lines (47-51). Data from Skoulidis *et al.* are *KRAS* mutants only.

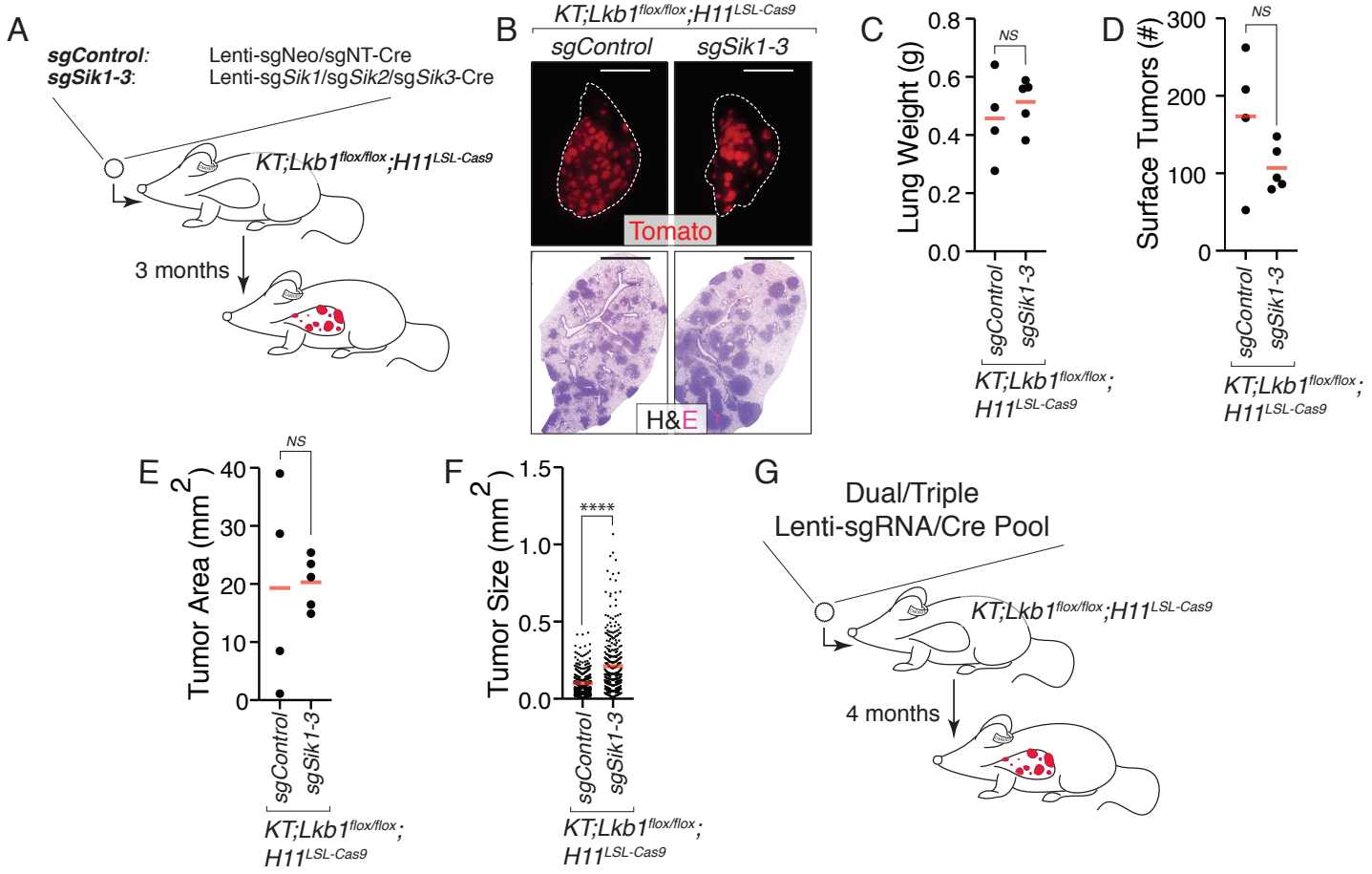

H

Vector	KT;Lkb1flox/flox;H11LSL-Cas9 95th Percentile (relative to Inerts)	FDR
sgNeo1-sgNT	0.98 ± 0.06	8.73E-01
sgNeo1-sgNT-sgNeo2	0.99 ± 0.20	9.79E-01
sgLkb1 1st-sgNT	1.21 ± 0.15	3.23E-01
sgLkb1 2nd-sgNT	1.14 ± 0.16	5.52E-01
sgNeo1-sgNT-sgLkb1 1st	0.74 ± 0.17	3.15E-01
sgNeo1-sgNT-sgLkb1 2nd	1.12 ± 0.28	7.90E-01
sgSik1 1st-sgNT	1.17 ± 0.25	6.96E-01
sgSik1 2nd-sgNT	1.63 ± 0.30	1.14E-01
sgSik3 1st-sgNT	1.63 ± 0.32	1.53E-01
sgSik3 2nd-sgNT	1.43 ± 0.52	6.11E-01
sgSik1 1st-sgSik3 1st	**3.32 ± 0.55**	**3.25E-04**
sgSik1 2nd-sgSik3 1st	**5.12 ± 0.82**	**3.06E-05**
sgSik1 1st-sgSik3 2nd	**2.67 ± 0.44**	**1.31E-03**
sgSik1 2nd-sgSik3 2nd	1.62 ± 0.98	7.27E-01
sgSik1 1st-sgSik2-sgSik3 1st	**2.91 ± 0.60**	**9.37E-03**

I

Vector	KT;Lkb1flox/flox;H11LSL-Cas9 LN Mean (relative to Inerts)	FDR
sgNeo1-sgNT	1.01 ± 0.07	9.37E-01
sgNeo1-sgNT-sgNeo2	0.98 ± 0.15	9.37E-01
sgLkb1 1st-sgNT	**1.50 ± 0.20**	**3.84E-02**
sgLkb1 2nd-sgNT	1.11 ± 0.18	6.85E-01
sgNeo1-sgNT-sgLkb1 1st	0.80 ± 0.15	2.97E-01
sgNeo1-sgNT-sgLkb1 2nd	1.29 ± 0.26	3.66E-01
sgSik1 1st-sgNT	1.25 ± 0.22	3.66E-01
sgSik1 2nd-sgNT	1.61 ± 0.31	1.53E-01
sgSik3 1st-sgNT	1.36 ± 0.28	2.97E-01
sgSik3 2nd-sgNT	1.59 ± 0.34	2.10E-01
sgSik1 1st-sgSik3 1st	**4.01 ± 0.75**	**3.86E-04**
sgSik1 2nd-sgSik3 1st	**7.09 ± 1.31**	**9.37E-05**
sgSik1 1st-sgSik3 2nd	**3.56 ± 0.75**	**3.22E-03**
sgSik1 2nd-sgSik3 2nd	1.29 ± 0.26	6.89E-01
sgSik1 1st-sgSik2-sgSik3 1st	**3.21 ± 0.75**	**1.50E-02**

Supplementary Figure S11. Sik-mediated tumor suppression is partially retained in the absence of Lkb1.
A. Outline of CRISPR/Cas9-mediated inactivation of Siks in an Lkb1-deficient setting. Tumors were initiated in *KT* and *KT;Lkb1*$^{flox/flox}$*;H11*$^{LSL\text{-}Cas9}$ mice with the indicated Lenti-sgRNA/Cre vectors.
B. Representative fluorescence (top) and H&E (bottom) images of lungs from *KT;Lkb1*$^{flox/flox}$*;H11*$^{LSL\text{-}Cas9}$ mice after tumor initiation with the indicated Lenti-sgRNA/Cre vectors. Lung lobes are outlined in white. Top scale bars = 5 mm. Bottom scale bars = 2 mm.
C. Tumor burden represented as lung weight. Each dot represents a mouse. The crossbars indicate the mean.
D. Number of Tomato^{positive} surface tumors (>1 mm in diameter) detected. Each dot represents a mouse. Crossbars indicate the mean.
E-F. Total tumor area (**E**) and tumor size (**F**) from histology of *KT;Lkb1*$^{flox/flox}$*;H11*$^{LSL\text{-}Cas9}$ mice with tumors initiated by Lenti-sgRNA/Cre as indicated. Each dot represents a mouse (**E**) or a tumor (**F**). The crossbars indicate the mean. ****p-value <0.0001.
G. Experimental outline to quantify Sik-mediated tumor suppression in Lkb1-deficient context using Tuba-seq. Tumors were initiated in eight *KT;Lkb1*$^{flox/flox}$*;H11*$^{LSL\text{-}Cas9}$ mice using the pool of dual/triple Lenti-sgRNA/Cre vectors described in Figure 3A.
H,I. Summaries of tumor size relative to tumors initiated with either sgNeo1-sgNT and sgNeo1-sgNT-Neo2. Size comparisons for a series of Lkb1 and Sik-targeting sgRNA are reported in terms of maximum likelihood estimates and associated 95% confidence intervals for 95th percentile (**H**) or log-normal mean (**I**). Emboldened, red-colored vectors significantly increased the LN mean relative to inert vectors. Benjamini-Hochberg-corrected, bootstrapped P-values are shown.

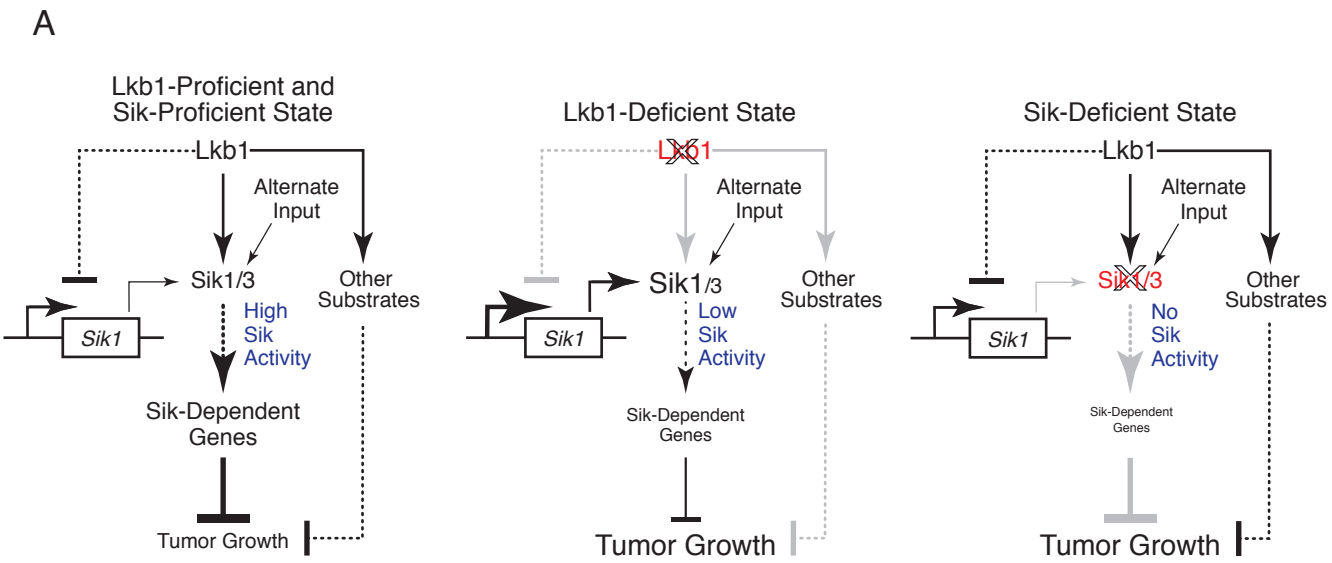

Supplementary Figure S12. Proposed model for an Lkb1-Sik axis of tumor suppresion
A. Schematic depicting proposed model for an Lkb1-Sik axis of tumor suppression. In the Lkb1-and Sik-proficient state, Lkb1 promotes the activity of Sik1/3, which alters Sik dependent genes and reduces lung tumor growth. Besides Siks, Lkb1 may also promote the activity of other tumor-suppressive substrates that remain to be identified. Upon Lkb1 inactivation, Sik1/3 activity, either kinase-dependent or independent, is reduced to residual levels maintained by an alternate minor upstream input and offset by increased Sik1 expression. This results in intermediate changes in the expression of Sik-dependent genes, which consequently promotes tumor growth. In contrast, in the Sik-deficient state, Sik activity is completely lost, which results in more dramatic changes in expression of Sik-dependent genes, and the net effect on tumor growth is comparable to, or greater than that of Lkb1 loss.